

1 **A morpho-tectonic approach to the study of earthquakes in Rome**

2
3 Fabrizio Marra^{1*}, Alberto Frepoli¹, Dario Gioia², Marcello Schiattarella³, Andrea
4 Tertulliani¹, Monica Bini⁴, Gaetano De Luca¹, Marco Luppichini⁵

5
6 ¹Istituto Nazionale di Geofisica e Vulcanologia, Via di Vigna Murata 605, 00143 Rome, Italy

7 ²Istituto di Scienze del Patrimonio Culturale (ISPC), Consiglio Nazionale delle Ricerche, Tito Scalo,
8 I-85050 Potenza, Italy

9 ³Dipartimento delle Culture Europee e del Mediterraneo (DiCEM), Università degli Studi della
10 Basilicata, I-75100 Matera, Italy; marcello.schiattarella@unibas.it

11 ⁴Dipartimento di Scienze della Terra, Università di Pisa, Italy

12 ⁵Dipartimento di Scienze della Terra, Università di Firenze, Italy

13
14 *corresponding author: fabrizio.marra@ingv.it

15
16 **Abstract**

17 Rome has the world's longest historical record of felt earthquakes, with more
18 than 100 events during the last 2,600 years. However, no destructive earthquake
19 has been reported in the sources and all of the greatest damage suffered in the
20 past has been attributed to far-field events. While this fact suggests that a
21 moderate seismotectonic regime characterizes the Rome area, no study has
22 provided a comprehensive explanation for the lack of strong earthquakes in the
23 region. Through the analysis of the focal mechanism and the morphostructural
24 setting of the epicentral area of a "typical" moderate earthquake (ML=3.3) that
25 recently occurred in the northern urban area of Rome, we demonstrate that this
26 event reactivated a buried segment of an ancient fault generated under both a
27 different and a stronger tectonic regime than that which is presently active. We
28 also show that the evident structural control over the drainage network in
29 this area reflects an extreme degree of fragmentation of a set of buried faults
30 generated under two competing stress fields throughout the Pleistocene. Small
31 faults and a present-day weaker tectonic regime with respect to that acting
32 during the Pleistocene **might explain the lack of strong seismicity in the long**
33 **historical record, suggesting that a large earthquake is not likely to occur.**
34 **explain the lack of strong seismicity and imply that a large earthquake could not**
35 **reasonably occur.**

36

37 **Key words:** Rome; geomorphology; streambed analysis; structural geology;
38 earthquakes; seismotectonics

39

40

41

42

43

44

45

46

47

48

49 **1. Introduction**

50 On May 11th 2020, a moderate ($M_L=3.3$, $Io= IV$ MCS) yet broadly felt earthquake
51 awoke most of the Rome's inhabitants at 05:03 a.m. (local time) (for details see
52 <https://e.hsit.it/24397691/index.html>). While producing no damage, the
53 shaking alarmed many citizens, who searched for information and reassurance
54 through the dedicated informative sources such as the INGV (Italian National
55 Institute of Geophysics and Volcanology) website. Others, instead, preferred to
56 trust on several popular beliefs which state that "Rome couldn't be struck by a
57 Big One" (i.e., a destructive earthquake with $M>7.0$), such as the mitigating effect
58 of the catacomb voids (trivial simplification from the Aristotelian theories), or
59 the protection granted by the Pope's presence. It is very likely that only few
60 people based their reactions upon a learned knowledge of the actual
61 seismotectonics features of the Rome's area. Indeed, even if a series of
62 specialized studies have been published in the last 20 years, a dedicated paper
63 investigating the reasons why Rome would not be affected by large earthquakes
64 is still missing in the scientific literature. Filling this gap is the aim of the present
65 paper in which we present a seismic study of the May 11th 2020 earthquake,
66 coupled with a statistical analysis of streambed directions in the epicentral area.
67 We identify the geometry of the seismogenic structure responsible for this $M=3.3$

68 event, and we frame it within the overall geo-morpho-structural setting of the
 69 Rome's area, providing insights on the seismo-tectonic features of this region.

70

71 **2. Seismicity of the Rome's area**

72 Our knowledge on the earthquakes that affected the roman area can be resumed
 73 from the seismic catalogues' records (Guidoboni et al., 2018; Rovida et al., 2020
 74 and from the literature (e.g., Tertulliani and Riguzzi, 1995; Molin and Rossi,
 75 2004; Galli and Molin 2014; Tertulliani et al., 2020) as follows:

- 76 • very few events caused significant damage in the city (1349, 1703, 1915),
 77 according to the studies mentioned above; all these large earthquakes
 78 occurred in the Apennines mountain range;
- 79 • some other seismogenic areas surrounding Rome (e.g., the Colli Albani
 80 Volcanic District) generated events that caused moderate damage;
- 81 • the Province of Rome (hereafter GAR, is the present metropolitan area of
 82 Rome) is periodically affected by low to moderate magnitude local
 83 earthquakes which is not supposed to cause significant damage.
- 84 • Uncertain events. Catalogue records quote several earthquakes that
 85 provoked some damage in Rome (see table 1). Most of such events,
 86 occurred during the Roman Age and Early Middle Ages are poorly
 87 documented and therefore not localizable.

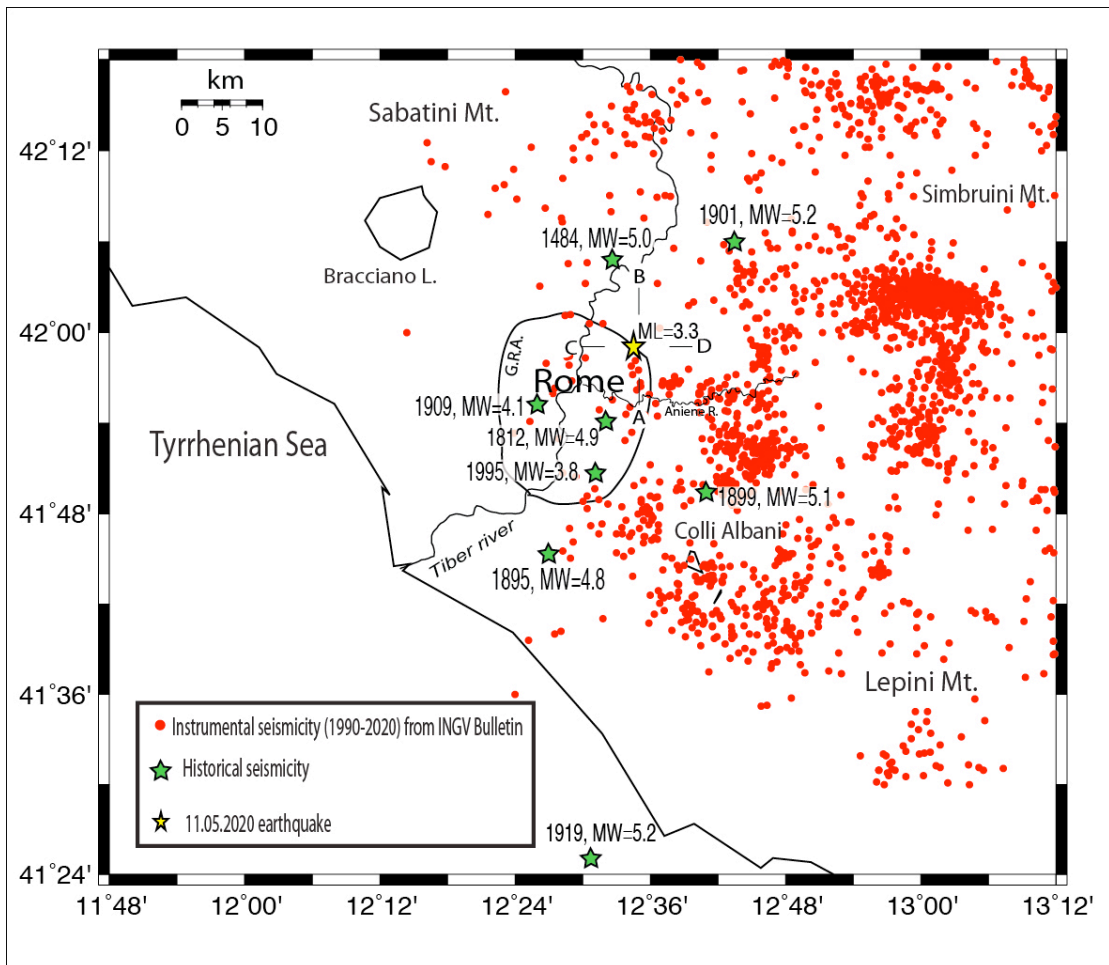
88 A summary of the historical and instrumental seismicity of the GAR is shown in
 89 Figure 1. Evidently, the completeness of our knowledge of seismicity decreases
 90 going back in time. In the period of ancient Rome, as well in the Early Middle
 91 Ages, strong earthquakes would seem hit Rome, sometime causing damage,
 92 whose origin is still unknown. The difficulty to understand if such earthquakes
 93 were generated by local or far-field sources depends on the documentary
 94 accounts: the earthquake was considered a prodigy, and as such, interpreted as a
 95 divine foretelling. Information on effects, damage or victims was often neglected,
 96 and very rarely documented. For these reasons we are not able to distinguish
 97 with reliability if such ancient events were originated, for example, in the
 98 Apennines region, or near Rome (in italic in table 1). In table 1 the earthquakes
 99 that hit Rome with a local intensity greater than 6 are listed.

100

Int. in Rome	Year	Epicentral Area	Epic Int Io	Mw
7-8	<i>83 BC</i>	<i>Rome</i>	7-8	5.4
7-8	<i>72 BC</i>	<i>Rome</i>	7-8	5.4
7-8	<i>15</i>	<i>Rome</i>	7-8	5.4
8	<i>51</i>	<i>Rome</i>	8	5.6
8	<i>443</i>	<i>Rome</i>	8	5.6
7-8	<i>484</i>	<i>Rome</i>	7-8	5.4
7-8	<i>801</i>	<i>Rome</i>	7-8	5.4
7	<i>1091</i>	<i>Rome</i>	7	5.1
7-8	<i>1349</i>	Central Apennines	9	6.3
5-6	<i>1703</i>	Central Apennines	11	6.9
6	<i>1703</i>	Central Apennines	10	6.7
6	<i>1730</i>	Central Apennines	9	6.0
6-7	<i>1812</i>	Rome	6-7	4.9
5-6	<i>1895</i>	Rome	6-7	4.8
6-7	<i>1899</i>	Albani Hills	7	5.1
6-7	<i>1915</i>	Central Apennines	11	7.1
6	<i>1927</i>	Albani Hills	7	4.9

101 Table 1. List of earthquakes that caused documented damage in the present GAR.
 102 The oldest events (italic in table) are not constrainable. (Data from Guidoboni et
 103 al., 2018; Rovida et al., 2021; Tertulliani et al.; 2020).

104
 105 It is interesting to note, from the seismic hazard point of view, that the epicenter
 106 of several more constrainable historical events, that occurred in the Roman
 107 countryside, are nowadays included in the GAR territory, densely urbanized.
 108 Within this limited territory we can anyway discriminate some different clusters
 109 of seismicity, in particular SE and NE of the City center. Of the first cluster are
 110 part the 1812, 1895, 1995 earthquakes, while the 1901 and 2020 events are
 111 located NE of the city (Figure 1). Very likely this seismicity feature is due to the
 112 activity of different seismotectonic structures.



113
114 **2. Seismotectonic features of the Rome's area**

115 Our knowledge on the earthquakes that affected the roman area can be resumed
116 from the seismic catalogues' records (Guidoboni et al., 2018; Rovida et al., 2020
117 and from the literature (e.g., Tertulliani and Riguzzi, 1995; Molin and Rossi,
118 2004; Galli and Molin 2014; Tertulliani et al., 2020) as follows:

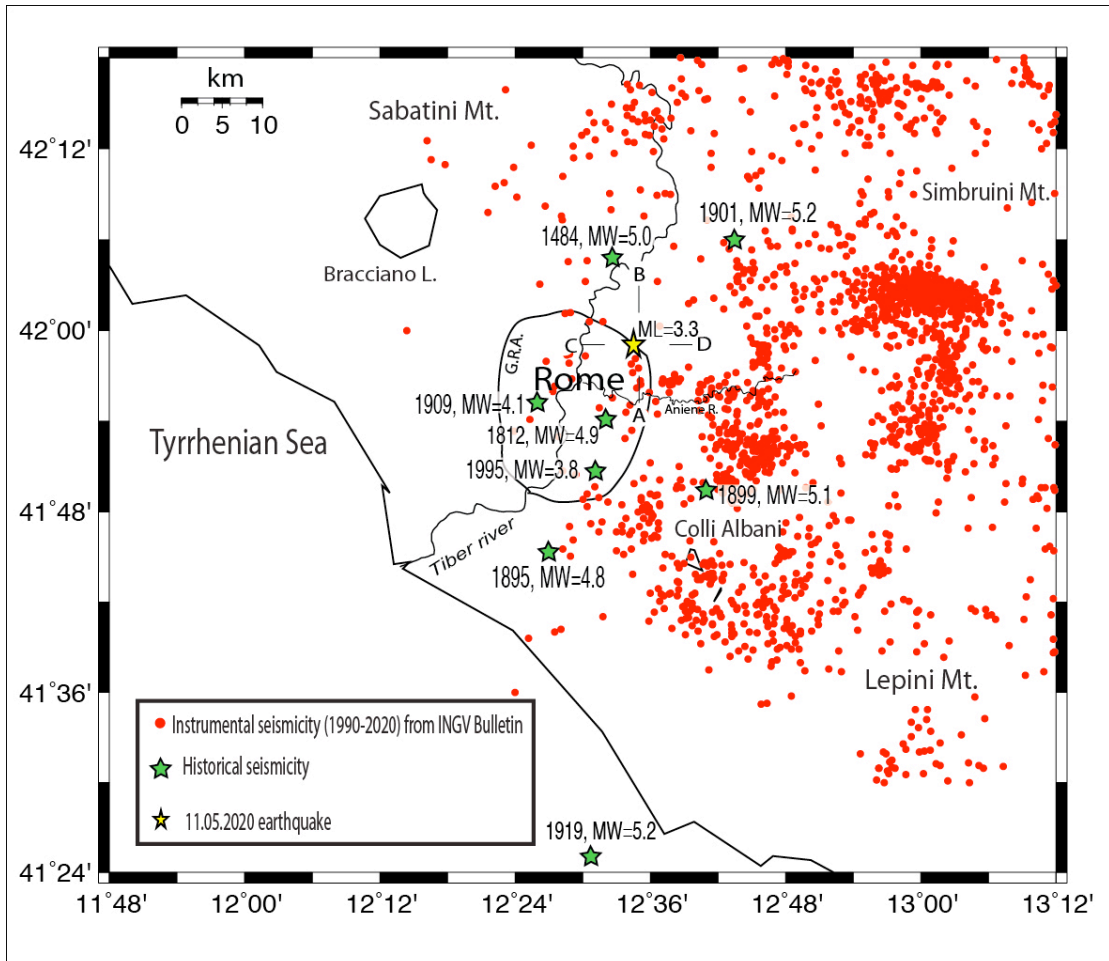
- 119 • very few events caused significant damage in the city (1349, 1703, 1915),
120 according to the studies mentioned above; all these large earthquakes
121 occurred in the Apennines mountain range;
- 122 • some other seismogenic areas surrounding Rome (e.g., the Colli Albani
123 Volcanic District) generated events that caused moderate damage;
- 124 • the greater area of Rome is periodically affected by low to moderate
125 magnitude local earthquakes which is not supposed to cause significant
126 damage.

127 A summary of the historical and instrumental seismicity of the grater area of
128 Rome is shown in Figure 1. Evidently, the completeness of our knowledge of
129 seismicity decreases going back in time. In the period of ancient Rome, as well in

130 ~~the Early Middle Ages, strong earthquakes would seem hit Rome, sometime~~
131 ~~causing damage, whose origin is still unknown. The difficulty to understand if~~
132 ~~such earthquakes were generated by local or far-field sources depends on the~~
133 ~~documentary accounts: the earthquake was considered a prodigy, and as such,~~
134 ~~interpreted as a divine foretelling. Information on effects, damage or victims was~~
135 ~~often neglected, and very rarely documented. For these reasons we are not able~~
136 ~~to distinguish with reliability if such ancient events were originated, for example,~~
137 ~~in the Apennines region, or near Rome.~~

138 ~~It is interesting to note, from the seismic hazard point of view, that the epicenter~~
139 ~~of several historical events, that occurred in the Roman countryside, are~~
140 ~~nowadays included in the greater Rome territory, densely urbanized.~~

141 ~~Within this limited territory we can anyway discriminate some different clusters~~
142 ~~of seismicity, in particular SE and NE of the City center. Of the first cluster are~~
143 ~~part the 1812, 1895, 1995 earthquakes, while the 1901 and 2020 events are~~
144 ~~located NE of the city (Figure 1). Very likely this seismicity feature is due to the~~
145 ~~activity of different seismotectonic structures.~~



146

147 **Figure 1.** Map showing the seismicity of the Rome's area and mainshock location (blue star) of
 148 the 11.05.2020 earthquake. A-B and C-D are the cross-sections in Figure 4b. G.R.A. is the beltway
 149 around Rome.

150

151 **3. Regional tectonic setting**

152 In approaching the geodynamics of this region the contribution of three main
 153 mechanisms of deformation should be considered, as proposed in Faccenna et al.
 154 (1996):

- 155 i) the NW-SE shortening (arrow #1 in Figure 2b) induced by the convergence of
 156 Africa and Europe (Tapponier, 1977);
- 157 ii) the sinking of the Ionian slab (arrow #2 in Figure 2b), producing the eastward
 158 migration (arrow #3) of the Apennine arc, and consequent back-arc extension
 159 (arrow #4) in the Tyrrhenian region (Malinverno and Ryan, 1986; Patacca and
 160 Scandone, 1989);
- 161 iii) the gravitational spreading of the overthickened crust (arrow #5 in Figure
 162 2b) in the Apennine crustal wedge (Reutter et al., 1980; Horvath and
 163 Berckhemer, 1982).

164 All these mechanisms are to be considered presently active in the Northern
 165 Apenninic arc on the basis of seismic and stress-field indications (Selvaggi and
 166 Amato, 1992; Amato et al., 1993; Frepoli and Amato, 1997; Mariucci et al., 1999;
 167 Luente and Speranza, 2001; Montone and Mariucci, 2016). Moreover, crustal
 168 thinning induced by extension was coupled with asthenospheric bulging (arrows
 169 #6 in Figure 2b), leading to the back-arc volcanism on the Tyrrhenian margin
 170 (Serri, 1997, and references therein). Such phenomena, and related magma
 171 underplating, enhanced the extensional processes (arrow #6' in Figure 2b) in a
 172 feedback mechanism in this region. In this regard, it is fundamental to notice that
 173 the Rome area and the Alban Hills are at the southeastern margin of the Latium
 174 Magmatic Province (Serri et al., 1993), and that very scanty volcanic activity
 175 occurred in the area between Rome and the Ortona-Roccamontfina Line (O-R in
 176 Figure 2a), which is considered (Patacca et al., 1990) a major geodynamic
 177 boundary separating the Central and Southern Apennines (Figure 2a). According
 178 to Marra (1999, 2001), the Sabina shear zone (Alfonsi et al., 1991) represents the
 179 northern boundary of this crustal disengagement zone. Based on its proximity to
 180 the Sabina shear zone, and in agreement with the numerous field evidence of
 181 fault kinematics (Faccenna et al., 1994a, 1994b; Marra, 2001; Marra et al., 2004)
 182 and the peculiar eruptive behaviour of the Alban Hills Volcanic District (Marra et
 183 al., 2009), Frepoli et al. (2010) proposed that the transpressional stress regime
 184 has been the prevailing one in this region during Quaternary times, and that it is
 185 temporarily superimposed by the extensional regime during periods of incoming
 186 volcanic activity and/or increased extensional activity (depending on which is to
 187 be considered cause and which effect) on the Tyrrhenian margin (Figure 2b).

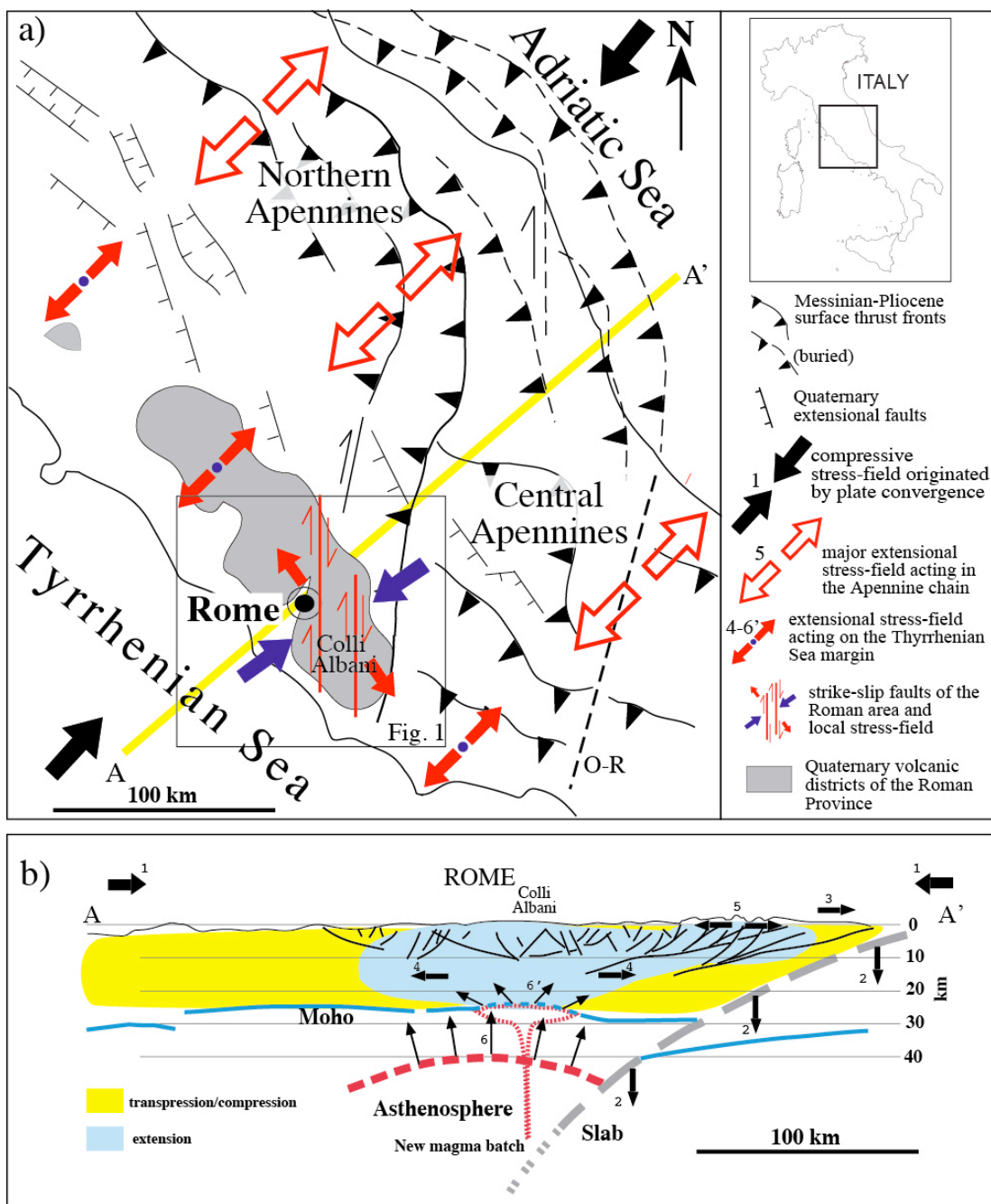
188
 189

190 **34. Morpho-structural features of the Rome's area**

191 The morpho-structural setting of the Roman area originates in the deformation
 192 of the geological substrate by combined faulting processes and erosion of rivers
 193 and streams (Del Monte et al., 2016). Although partially obliterated by millennia
 194 of anthropic interventions, it presents some evident and peculiar traits, whose
 195 analysis allows us to understand the features of the tectonic forces (and related
 196 stress-fields) that acted in the geological past through present time (Marra,

197 2001) (Fig. 2). Such analysis also consents to interpret the origin of the
 198 earthquakes that nowadays affect this area.

199



200
 201 **Figure 2.** Structural scheme of central Italy showing the competing tectonic force fields and the
 202 main faults associated with them that acted in the Middle-Upper Pleistocene. See text for
 203 comments and explanations.

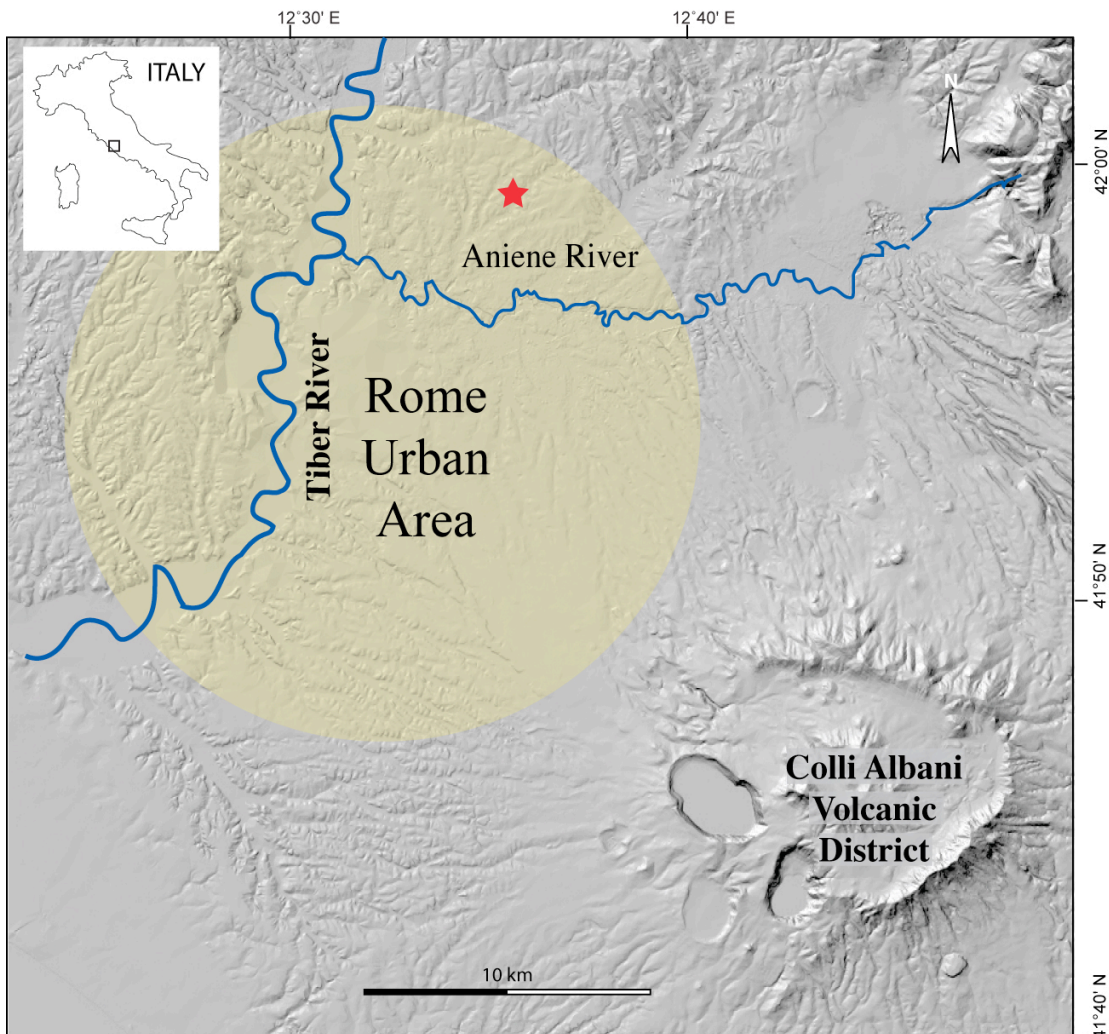
204

205

206 If we could see what the topography was like before the foundation of the City,
 207 the area of Rome would appear as a large flat sector, deeply engraved and
 208 dissected by the valleys of the tributary streams of the Tiber and Aniene Rivers,

209 and by the wider ones of the two main watercourses. While these features are
 210 less visible in the historical center of Rome, they are still well recognizable
 211 through a Digital Elevation Model (DEM) in its surrounding territory, as
 212 highlighted in Fig. 3.

213



214
 215 **Figure 3.** Digital elevation model (DEM) of the Roman area (TINITALY by Istituto Nazionale di
 216 Geofisica e Vulcanologia (INGV), published with a CC BY 4.0 license; available at:
 217 <https://doi.org/10.13127/TINITALY/1.0>), showing the strongly marked characters of the river
 218 and stream incisions that form the hydrographic network afferent to the Tiber and the Aniene
 219 Rivers. Location of the 10.05.2020 earthquake is also shown (red star).

220

221

222 Most of the tabular surface highlighted by the shaded area in Fig. 3 is a
 223 "pyroclastic plateau" created by the emplacement of large coulters of volcanic
 224 deposits **erupted from the Colli Albani and Monti Sabatini districts**. These are
 225 represented by pyroclastic flows, originated by the collapse of the sustained
 226 eruptive column, and air-fall products such as windblown pumice, scoria and

227 lapilli. The deposition of these volcanic products, starting from around 600,000
228 years ago (Marra et al., 2014; Gaeta et al., 2016), leveled the ground creating a
229 thick, layered blanket of sediments which was soon after etched by the erosive
230 action of the watercourses. The latter, however, did not settle at random, but
231 progressively shifted in correspondence with embryonic fractures and fault lines
232 created by active tectonic deformation. The same fracturing and faulting
233 associated with the extensional tectonic regime which shaped the Tyrrhenian
234 Sea margin of central Italy during the Pleistocene allowed the magma residing in
235 the mantle to rise to the surface (e.g., Locardi et al., 1977, Acocella and Funiciello,
236 2006), originating the volcanoes of the so-called "Roman Province" (Peccerillo,
237 2017) (Fig. 2). An intense seismotectonic regime must have been associated to
238 these large extensional faults, likely producing strong earthquakes throughout
239 this region.

240
241 From the end of the Middle Pleistocene (125,000 years ago), the tectonic activity
242 began to decrease in intensity, paralleling the decrease in volcanic activity
243 (Marra et al., 2004a). Hence the seismogenic potential of the faults associated
244 with this tectonic regime must also have decreased significantly. This is one of
245 the reasons why Rome is today a low seismicity area. Moderate earthquakes
246 ($M \leq 5.0$) (Tertulliani and Riguzzi, 1995; Basili et al., 1995) are almost exclusively
247 concentrated in the volcanic area of Colli Albani (Amato and Chiarabba, 1995),
248 which is in a quiescent status (Trasatti et al., 2018). The moderate seismicity of
249 the Roman area reflects an active stress-field of the same nature, but weaker,
250 than the extensive tectonic regime that characterized the Tyrrhenian Sea margin
251 of central Italy for the entire Pleistocene, as revealed by the study of the focal
252 mechanisms of these earthquakes and borehole breakouts (Montone et al., 1995;
253 Montone and Mariucci, 2016). Such weaker tectonic regime, therefore,
254 reactivates all the faults present in this region with small movements, compatible
255 with their orientation with respect to the vectors of the stress-field (Frepoli et al.,
256 2010). The seismic events associated with this regime do not generate ground
257 ruptures, as it happens for strong, heavy damaging earthquakes, because the
258 small displacements that occur on the fault planes at depth do not propagate to
259 the surface. However, these movements repeated over time generate a slow and

260 progressive deformation of the soil, conditioning the flow direction of surface
261 waters, and exerting a "structural control" on the stream axes and alluvial valleys
262 (Marra, 2001). It follows that the hydrographic network has assumed over time a
263 geometry reflecting that of the faults occurring in the geological substrate.

264

265

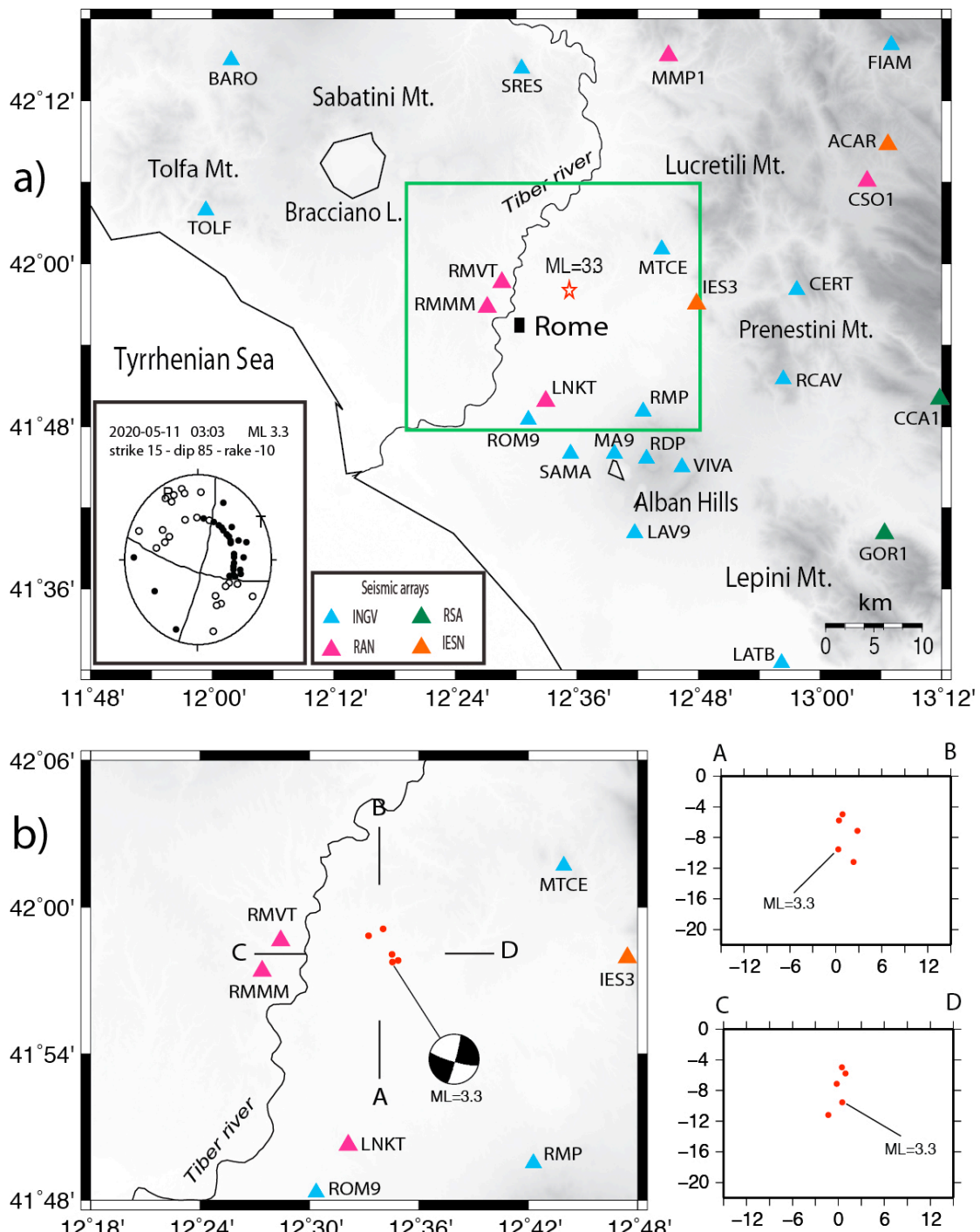
266 **5. Data and Methods**

267 **5.1 Seismic analysis**

268 **4. Seismicity**

269 The small seismic sequence occurred on May 11th 2020 in the north-eastern area
270 of Rome was recorded by the Italian National Seismic Network (RSN) of the
271 Istituto Nazionale di Geofisica e Vulcanologia (INGV) and by the regional seismic
272 network of Lazio and Abruzzo (RSA) (De Luca et al., 2009; Frepoli et al., 2017)
273 (Figure 4). Both national and regional Italian seismic networks have been
274 significantly extended in the last two decades through installation of new three
275 components, mostly broadband, stations. In addition we integrated the dataset of
276 this sequence with the data of the Italian strong motions network (RAN)
277 **operated by the National Civil Protection Department** and with the IESN network
278 (Italian Experimental Seismic Network) of Central Italy, an amateur seismic
279 network equipped with very good digitizers and sensors. This dense monitoring
280 improved in the last decade the detection and location of the seismicity in central
281 Italy.

282 To accurately relocate the seismicity, we used the Hypoellipse code (Lahr, 1989)
283 and a reliable 1D V_p velocity model computed by the application of a genetic
284 algorithm (Holland, 1975; Sambridge and Gallagher, 1993). A constant value of
285 1.84 V_p/V_s determined with the Wadati method (Chatelain, 1978) was used.



286

287 **Figure 4.** a) Distribution of the seismic stations of the Italian National Seismic Network (RSN) of
 288 the Istituto Nazionale di Geofisica e Vulcanologia (INGV) and of the regional seismic network of
 289 Lazio and Abruzzo (RSA) used to locate the epicenter of the 11.05.2020 event (red star). b) Map
 290 and vertical distribution of the mainshock and two aftershocks.

291

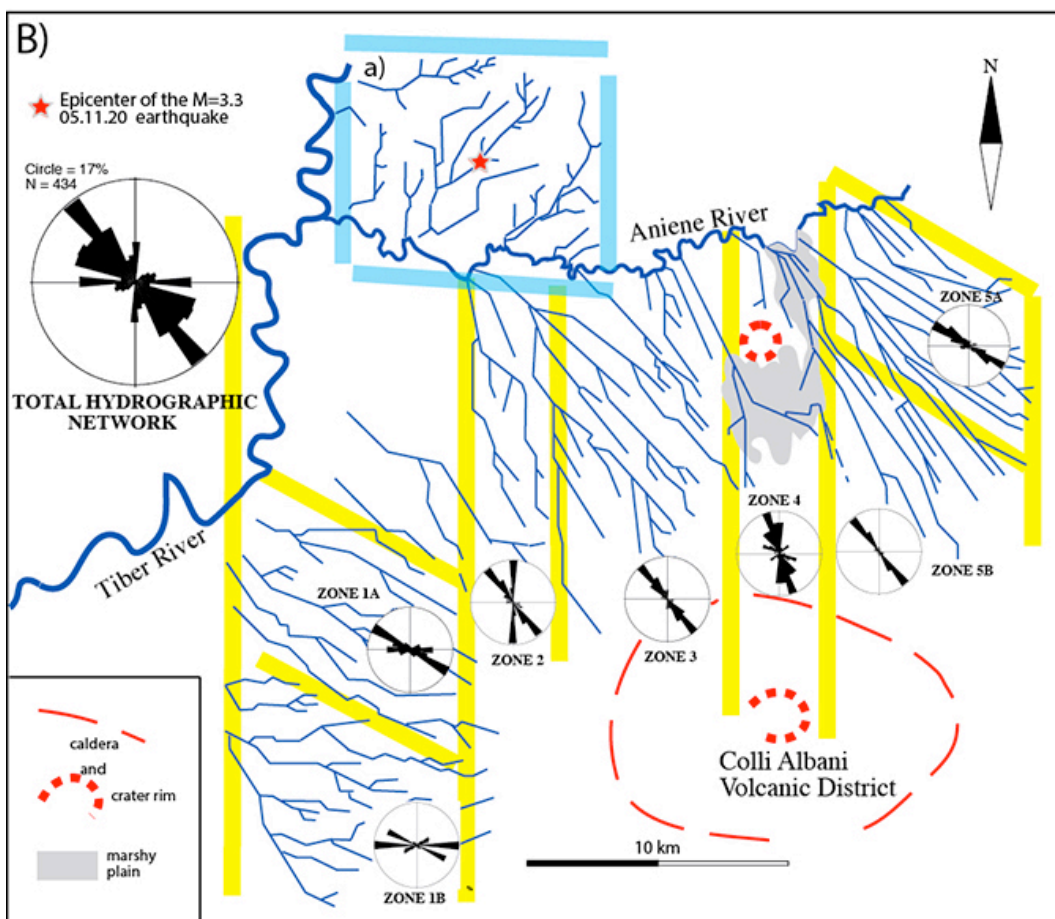
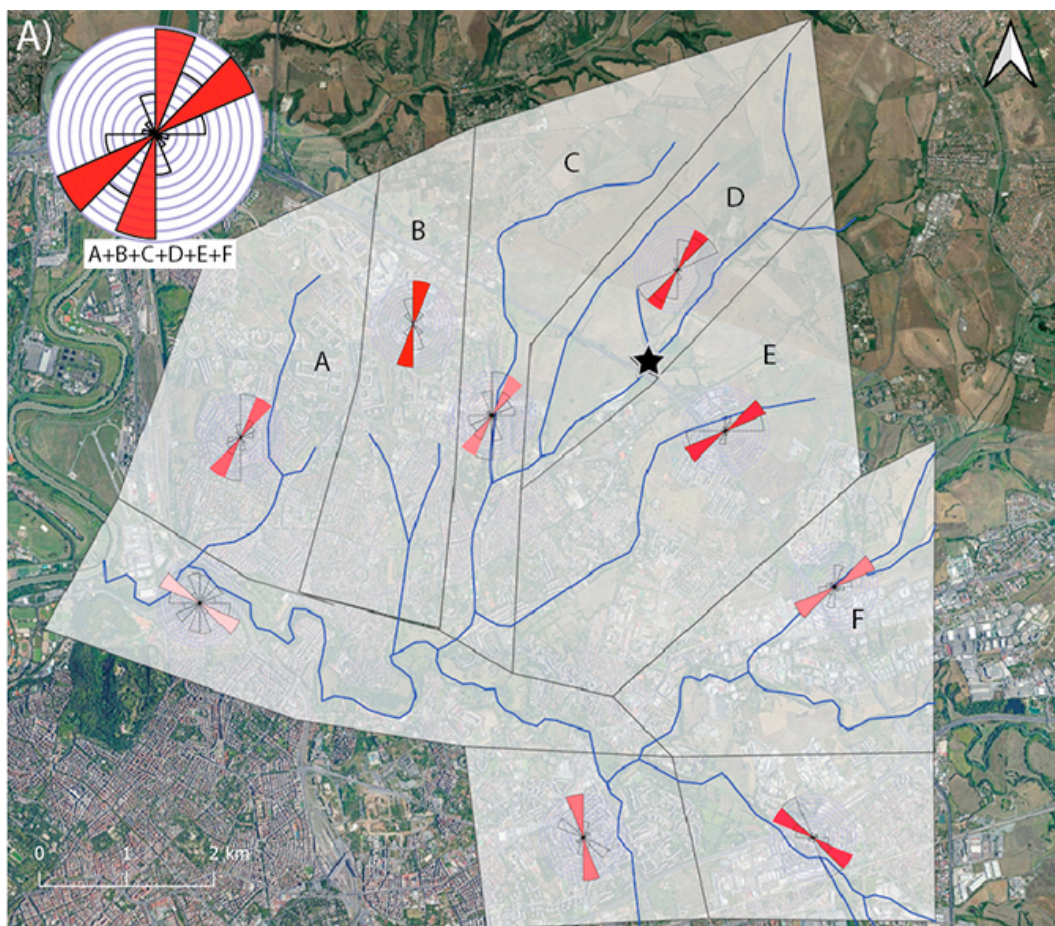
292 5.2 Geomorphology

293 5.2.1 Previous studies

294 A quantitative analysis of drainage trends in the south-eastern area of Rome
 295 bounded by the Tiber and Aniene Rivers and by the Colli Albani volcanic district

296 was carried ~~on-out~~ by Marra (2001). A simple technique based on statistical
297 analysis of rectified directions of streambeds was applied- (e.g., Ciccacci et al.,
298 1987; Caputo et al., 1993; Macka, 2003). Stream channel directions for the total
299 area and for different sectors were weighted according to three groups of length,
300 independent of hydrographic order, and plotted on rose diagrams.
301 While it is possible that rectifying drainage patterns can introduce directionality
302 that is unrelated to structural control, it still does indicate preferential directions
303 of river flow. In the case that these preferential directions of river flow were
304 statistically significant and different from those expected from non-structural
305 controls (e.g. topographic and geographic trends), they were interpreted to be
306 diagnostic of the structural setting. Anthropic intervention is also possible cause
307 of rectification of water channels, however, the linearity of the alluvial valleys
308 forming in the hydrographic network consents to compare and support the
309 directionality of the streambeds. Indeed, deep incisions and a "canyon-like"
310 morphology characterizes the alluvial plains forming the hydrographic network
311 (see Fig. 3), due to the occurrence of ca. 50 m tectonic uplift in the last 250 ka
312 (Marra et al., 2016).

313



315 **Figure 5.** A) Result of the streambed direction analysis performed in this work
 316 within the hydrographic basin including the epicenter area of the May 11th event
 317 (pale-blue borders in B) is compared with that performed in the south-eastern
 318 Roman area, between the Tiber, the Aniene and the Colli Albani (B) (Marra,
 319 2001). **Yellow lines border the different sectors of the analyzed drainage**
 320 **catchment basins.** Analysis in the historical city center was hindered by the
 321 occurrence of a widespread anthropic cover. Basemap from Qgis
 322 QuickMapServices (available under [Creative Commons Attribution-ShareAlike](https://creativecommons.org/licenses/by-sa/3.0/)
 323 [3.0 licence \(CC BY-SA\)](https://creativecommons.org/licenses/by-sa/3.0/) at:
 324 https://plugins.qgis.org/plugins/quick_map_services/).

325
 326 Results of the analysis conducted by Marra (2001) are shown in Fig. 5B showing
 327 that the NW-SE direction is the dominant one in the total area analysis (large
 328 diagram in the left upper corner), as opposed to an expected radial drainage
 329 trend descending from the Colli Albani caldera rim **and affecting an**
 330 **heterogeneous geologic substrate.** The maximum concentration of fluvial
 331 channel directions oriented $N145^\circ$ matches the strike of extension-induced faults
 332 and fractures and agrees with the present-day stress field determined from focal
 333 mechanisms and breakouts data in this region (Montone et al., 1995; Montone
 334 and Mariucci, 2016). Moreover, there are significantly different concentrations in
 335 discrete sectors delimited by the yellow lines. In particular, there are two narrow
 336 bands (zones 2 and 4) where the N-S direction of the streambeds prevails, and
 337 peculiar "domains" (zones 1A, 5A) where the WNW-ESE one is prevailing. The
 338 validation of the 'tectonic' hypothesis was performed through comparison with
 339 geometry and kinematics of fault and fractures surveyed in the area, allowing
 340 to interpret the pattern highlighted as the result of a complex structural control
 341 in this area, exerted by two competing stress-fields alternating each other
 342 throughout Pleistocene times (Marra, 1999, 2001; Frepoli et al., 2010).
 343

344 **5.2-3 Streambed analysis**

345 In order to compare the results with previous analysis of the regional
 346 deformation pattern, a quantitative analysis of drainage trends has been
 347 performed in the discrete hydrographic basin located in the sector NE of the
 348 Tiber and Aniene Rivers confluence (Fig. 5A), within which the May 11th
 349 earthquake occurred.

350 The streambed direction analysis within the hydrographic basin including the
 351 epicenter area of the May 11th event was created by using the QGIS "Line
 352 Direction Histogram" plugin (Tveite, 2015), that visualizes the distribution of
 353 line segment directions as a rose diagram (weighted using the line segment

354 lengths). The number of bin of direction which composes the rose diagram could
355 be set and in this work we used 8 bins corresponding to the main cardinal
356 directions. The tiles in which the area has been divided were identified
357 according to the main directions of streambeds.

358

359 **5.3-4 Drainage network anomalies and river profile analysis**

360 Drainage network anomalies are one of the most useful morphotectonic
361 indicators of active tectonics and they are widely used as an effective tool to infer
362 the possible control of fault activity on landscape and channels (see for example,
363 Boulton et al., 2014; Calzolari et al., 2016; Pavano et al., 2016; Kent et al., 2017;
364 Baharami, 2013). Integrated studies of possible active tectonic control on the
365 geometry of the drainage network frequently include analysis of river
366 longitudinal profiles, preferential orientation and alignments of channels, right-
367 angle confluences and fluvial elbows (Boulton et al., 2014; Pavano et al., 2016;
368 Kent et al., 2017; Gioia et al., 2018). Indeed, river profile analysis is one of the
369 most powerful tools for the identification of transient state of a drainage
370 network and recognition of knickpoints/knickzones, which represent valuable
371 and effective morphotectonic markers of recent crustal deformation (Whipple
372 and Tucker, 1999). Our approach combines the analysis of anomalies in drainage
373 network geometry (i.e. preferential orientation and/or alignments of channels,
374 fluvial elbows, right-angle confluences) with the identification of
375 knickpoints/knickzones of tectonic origin in transient longitudinal river profiles.
376 Such data have been used as morphotectonic evidences of active/recent tectonic
377 deformation induced by fault system responsible for the seismic activity of the
378 study area.

379 River profile analysis has been carried out according to the methods and
380 procedures developed by Wobus et al. (2006), Forte and Whipple (2019) using a
381 DEM with a spatial resolution of 10 m. Stream profile analysis is classically
382 carried out by identifying knickpoints or knickzones along the river longitudinal
383 profiles or by extracting a linear regression in a log-log slope-area graph, which
384 allowed us to extrapolate the concavity index (the slope of the regression) and
385 the steepness index (the y-intercept, that is the projection of the best-fit line that
386 intersects the y-axis). Knickpoints or abrupt scarps of the longitudinal profiles

387 can be related to tectonic- or eustatic- induced perturbations of ancient base-
388 levels but their formation and migration can be also related to a co-seismic fault
389 ruptures **or deformation induced by blind faults** (Kirby and Whipple, 2012). In
390 particular, the identification of fault-induced disturbance on channel profiles can
391 be performed through the recognition of linear alignments of
392 knickpoints/knickzones in channels with different sizes and orientations
393 (Boulton et al., 2014; Kirby and Whipple, 2012).
394 In order to investigate the possible occurrence of fault-related knickpoints and
395 river profile anomalies, we have investigated the river longitudinal profiles of the
396 main channels of the study area through the identification and mapping of
397 abrupt changes in river profile shape. Such data have been combined with the
398 morphotectonic analysis of the spatial distribution of drainage network
399 anomalies. Then, their spatial distribution has been used to infer the traces of
400 possible tectonic lineaments of the study area.

401

402 **6. Results**403 **6.1 Focal mechanism and re-location of the 11 May earthquake**

404 The M_L 3.3 mainshock (11 May at 03:03 UTC) was followed over the next two
405 days by only four small aftershocks with magnitude ranging from 0.7 to 1.8
406 (**Table 2**). Thanks to the high station coverage we were able to determine all
407 earthquake hypocenter depths with acceptable uncertainties. The average
408 location errors are 0.14 km (horizontally) and 0.32 km (vertically) with a
409 confidence level of 90%. Mainshock hypocenter is at 9.6 km of depth, while the
410 aftershock hypocenters are ranging from 5.0 to 11.2 km of depth (Fig. 4). The
411 two largest aftershocks (magnitude M_L 1.8 and 1.4, respectively) have depth
412 between 5.0 and 5.8 km, and are located very close to the mainshock epicenter,
413 while the two smallest aftershocks (both magnitude M_L 0.7) are located slightly
414 towards NW with respect to the mainshock epicenter, at 7.2 and 11.2 km of
415 depth. **These two aftershocks are clearly unrelated with the seismogenic**
416 **structure responsible for the mainshock and are likely the effect of stress**
417 **propagation to a contiguous fault.**

418

419

420

421

422

423 **Table 2. List and localization parameters of the Rome sequence (May 2020).**

424

425

Date	Origin time	Lat	Lon	Depth	Azimuthal gap	RMS	Magnitude M_L
2020-05-11	03:03	41 57.77	12 34.54	9.6	44	0.14	3.3
2020-05-11	03:14:43	41 59.13	12 34.05	7.2	72	0.12	0.7
2020-05-11	03:14:47	41 58.84	12 33.25	11.2	73	0.11	0.7
2020-05-12	00:06	41 57.83	12 34.87	5.8	47	0.18	1.8
2020-05-13	00:07	41 58.08	12 34.53	5.0	46	0.20	1.4

426

427 We have computed the fault plane solution of the mainshock with the FPFIT code
 428 (Reasenberg and Oppenheimer, 1985). First-motion polarities are 57. The focal
 429 mechanism has a large strike-slip component (first nodal plane: strike 21015,
 430 dip 6585, rake -2510). T-axis is oriented in a NE-SW direction according with the
 431 general "Antiapennine" (NE-SW) extension. Following some tectonic information
 432 of this area, the fault plane coincides with the NNE-SSW nodal plane of the
 433 solution which has a left-lateral strike-slip kinematics.

434

435 **6.2 Statistical analysis of streambed directions in the epicenter area**

436 Results of the streambed analysis in the small hydrographic basin where the
 437 epicenter of the May 11th earthquake occurred are summarized in Fig. 5A.
 438 The streambeds in the eastern portion of the basin (discrete sectors D, E, F)
 439 concentrate around the NE-SW direction, which is the one expected based on the
 440 topographic gradient, perpendicular to the Aniene River course, towards which
 441 the catchment basin drains. In contrast, an abrupt rotation occurs in the western
 442 portion of the basin (discrete sectors A, B, C), where the streambeds are aligned
 443 along the NNE-SSW direction, parallel to the main watercourse of the Tiber
 444 River. Similarly to the results obtained in the southern area by Marra (2001),
 445 showing that the ca. N-S direction is a characteristic feature of the streambeds in
 446 this region which is clearly independent by the geographic and topographic
 447 control on the hydrographic network, we interpret the N-S lineaments to reflect
 448 tectonic control on the streambeds exerted by fault activity in the analyzed basin.
 449 As it has been remarked in previous works (e.g., Alfonsi et al., 1991; Faccenna et
 450 al., 1994, 2008; Marra et al., 2004b) strike-slip, right-lateral N-S faults have been

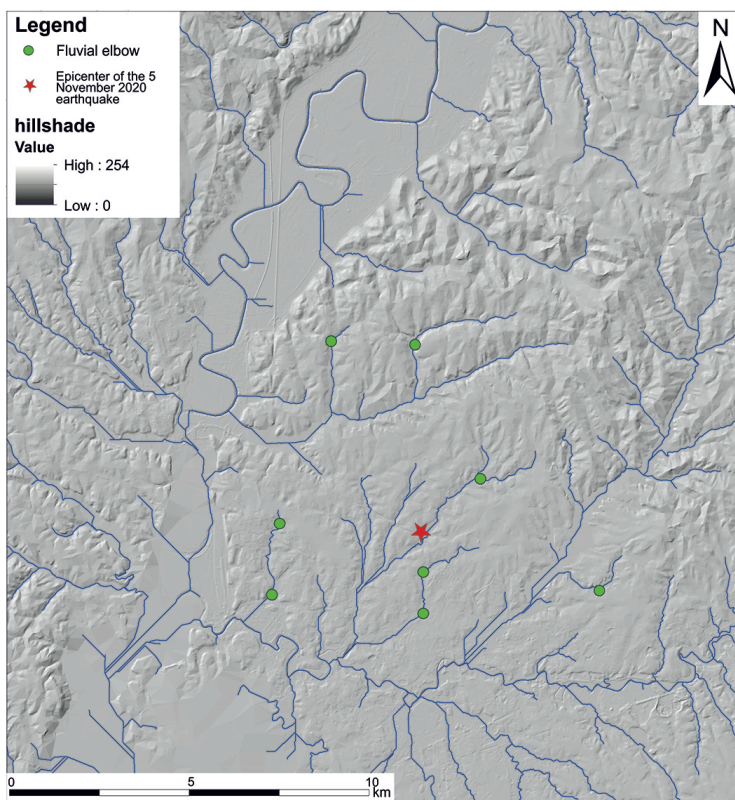
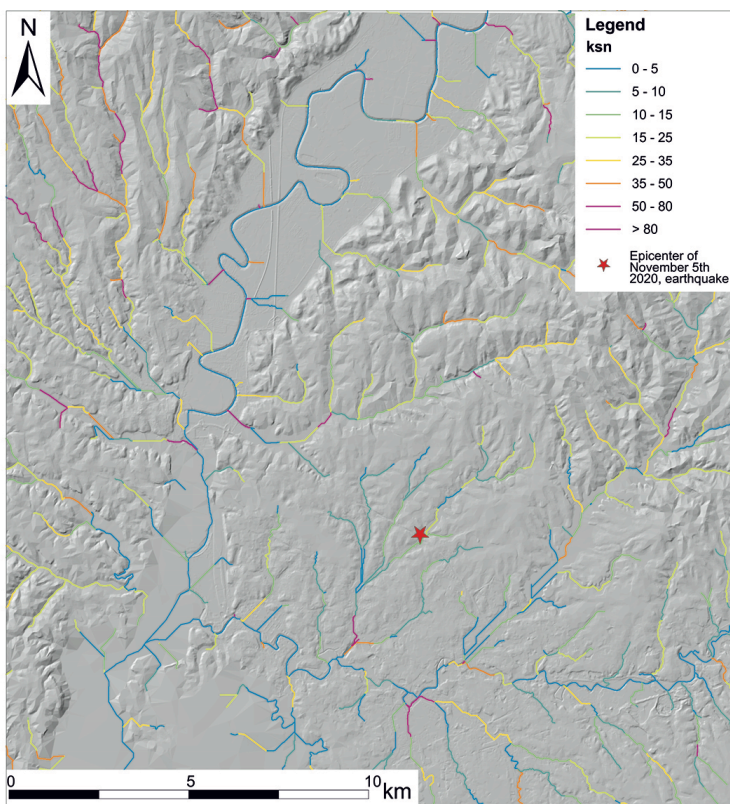
451 active repeatedly during the Pleistocene, up to historical times. Frepoli et al.
 452 (2010) have remarked on the direct relationship between the sectors
 453 characterized by N-S direction of the streambeds and seismically active fault
 454 zones. It is worth noting that the May 11th earthquake epicenter occurs on the
 455 northern continuation of one such N-S zone (zone 2 in Fig. 5B).

456

457 **6.3 Morphotectonic analysis of the drainage network: river profile analysis**
 458 **and drainage network anomalies**

459 Analysis of longitudinal river profiles of the bedrock-rivers is based on the
 460 stream power incision model (Whipple and Tucker, 1999; Wobus et al., 2006;
 461 Forte and Whipple, 2019) and has been carried out to evaluate the channel
 462 response to eustatic- and tectonic-induced processes. In a first step, we prepare a
 463 map of the normalized steepness index (ksn) with a reference concavity index of
 464 $\theta_{ref} = 0.45$ (Fig. 6a). Ksn map allowed us to perform a preliminary analysis of the
 465 spatial distribution of ksn values, which can be useful to individuate the sectors
 466 of the landscape featured by knickpoints and knickzones of tectonic origin.
 467 Moreover, a morphotectonic map showing the spatial distribution of fluvial
 468 elbows and anomalies in drainage network geometry was also introduced (Fig.
 469 64b). Fig. 7 shows the results of the analysis of the river profiles, which
 470 highlights how most of the channels deviates from the typical equilibrium shape
 471 of the longitudinal profiles. Longitudinal profiles are featured by the presence of
 472 knickpoints and knickzones, mainly in the central reach of the river profiles.
 473 These knickpoints appear not controlled by lithological contact and suggest a
 474 transient state of the fluvial net induced by tectonic perturbation or eustatic
 475 base-level variations. In particular, we detect the occurrence of convex zones or
 476 knickpoints related to a past base-levels, as testified by the presence of a large
 477 “terraced surfaces” at altitude ranging from 60 to 40 m a.s.l. (Fig. 7). Our analysis
 478 also reveals the occurrence of a cluster of knickpoints in the right-orographic
 479 side of the Aniene River with different features than the previous ones. In fact,
 480 they can be classified as slope-break knickpoint (*sensu* Wobus et al., 2006, see
 481 also Kirby and Whipple, 2012) and are aligned along NW-~~SO~~-SE and N-S
 482 orientation. Such alignments as well as the location of anomalous confluences
 483 and right-angle elbows of the drainage network allowed us to infer the

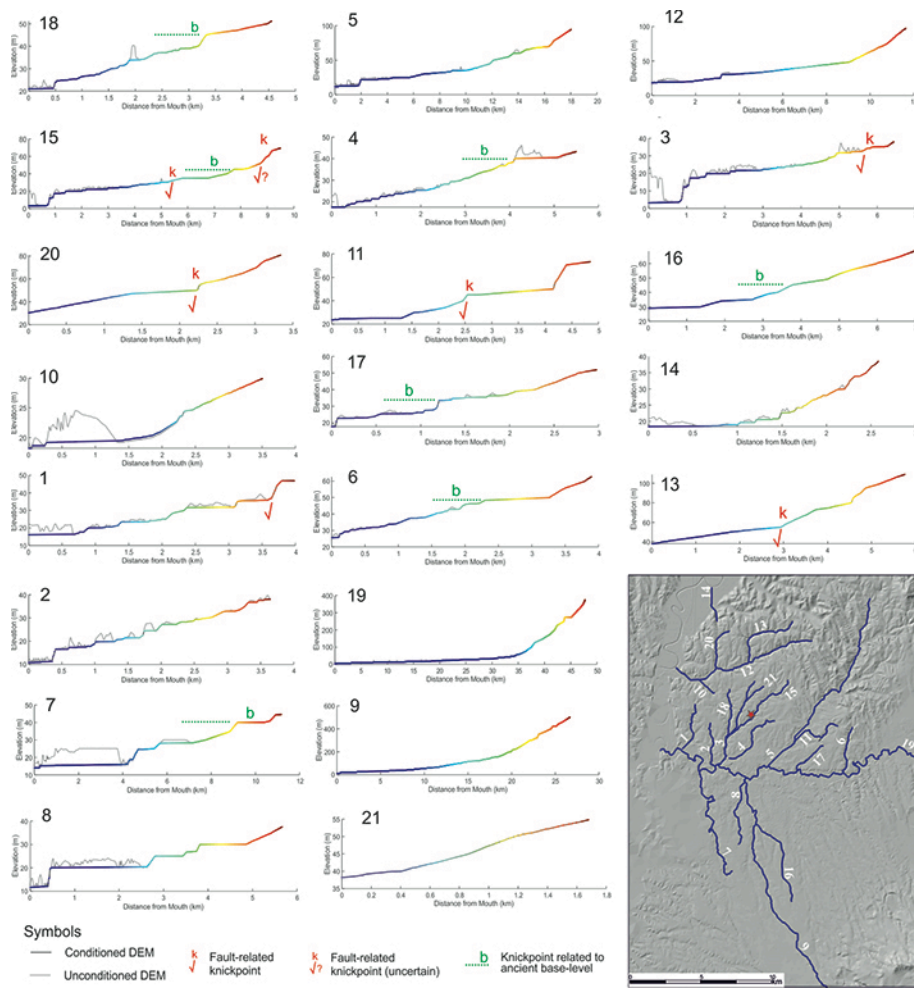
484 occurrence of the tectonic lineaments mapped in Fig. 78, which can be
 485 responsible for the recent tectonic activity that promoted the perturbation of the
 486 fluvial net.



487

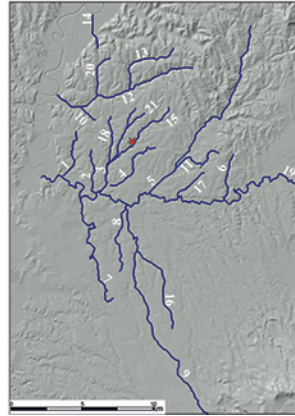
488
489
490
491
492
493

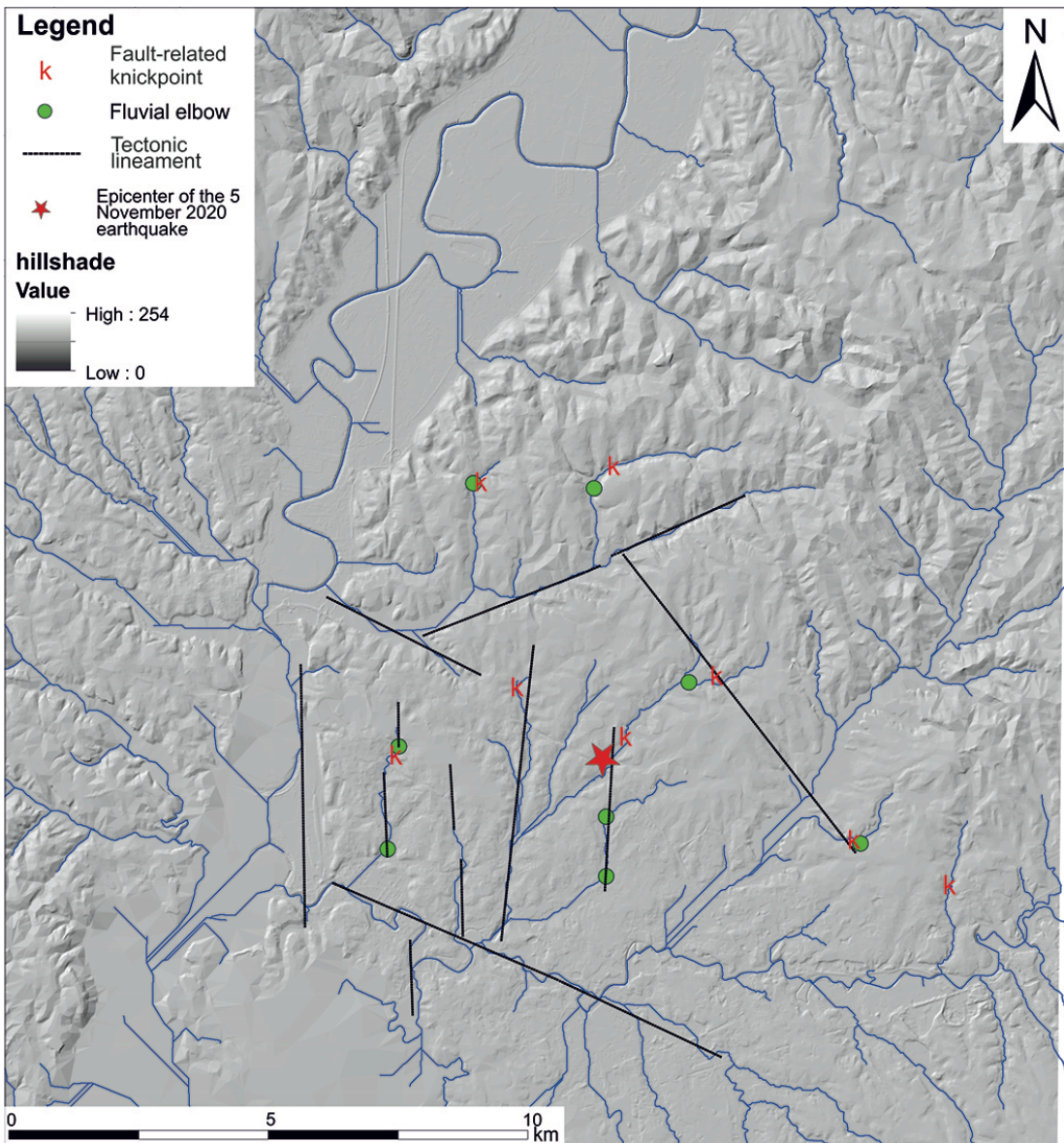
Figure 6. a) Hillshade of the study area and distribution of the normalized channel steepness
index (ksn , $\theta_{ref} = 0.45$); b) Drainage network of the study area and main planar anomalies of the
fluvial net. Tectonic lineaments inferred by morphotectonic analysis are also showed.



494
495
496
497

Figure 7. Longitudinal profiles of the main channels of the study area (location and numbering
in the main map) and interpretation of the knickpoints.





498
499 **Figure 8.** Tectonic lineaments of the study area inferred by morphotectonic analyses and the s
500 spatial distribution of the main drainage network anomalies of the study area (i.e. fluvial elbow
501 and knickpoints of river profiles). Hillshade was derived by the 10 m TINITALY DEM
502 DEM images in these figures: TINITALY, by published with a CC BY 4.0 license by Istituto
503 Nazionale di Geofisica e Vulcanologia (INGV), published with a CC BY 4.0 license; available at:
504 <https://doi.org/10.13127/TINITALY/1.0>.

505 7. Discussion

510 Studies conducted during the last two decades by the INGV on the geological-
511 structural and seismic-tectonic setting of the Roman area have shown that the
512 geometry of the hydrographic network reflects that of a set of buried faults
513 (Marra, 199, 2001; Frepoli et al., 2010). Considering the significant offsets
514 affecting the Middle-Pleistocene volcanic deposits in this area (e.g., Faccenna et

515 al., 1994a, 1994b; Marra, 2001) compared to the lack of strong events in the
516 historical record, it is inferred that these ~~These are~~ faults ~~that~~ are no longer
517 active with the seismic intensity they had in the geological past. We conclude
518 that ~~they~~They are reactivated under the effect of the stress-field that currently
519 acts in the upper crust and determines the genesis of low-magnitude
520 earthquakes in this region.

521 In particular, it has been shown that the ~~drainage network pattern directions of~~
522 ~~the streambeds and the distribution of river profile anomalies (i.e. fluvial elbows~~
523 ~~and knickpoint/knickzones)~~ reflect the deformation field induced on the surface
524 by the reactivation of these buried faults, with a set of three preferential
525 alignments:

526 i- The first displays an NW-SE "Apennine" direction, ("a" in Fig. 89), which
527 precisely reflects that of the large, dip-slip extensional faults that first created the
528 Tyrrhenian Sea marine basins (Barberi et al., 1994) and later, in the lower-
529 middle Pleistocene, the so-called "Tyrrhenian margin" (Fig. 2). This is a wide
530 hilly or sub-flat area between the Apennine chain and the present coast,
531 originated by the fault displacement and the "staircase" lowering of the
532 mountain relief (Parotto and Praturlon, 1975). The direction of these faults also
533 reflects the alignment of the volcanoes that developed in the Middle Pleistocene
534 along the Tyrrhenian margin, following the rise of magmas mainly along the
535 fractures in the earth's crust created by these tectonic structures (Locardi et al.,
536 1977).

537

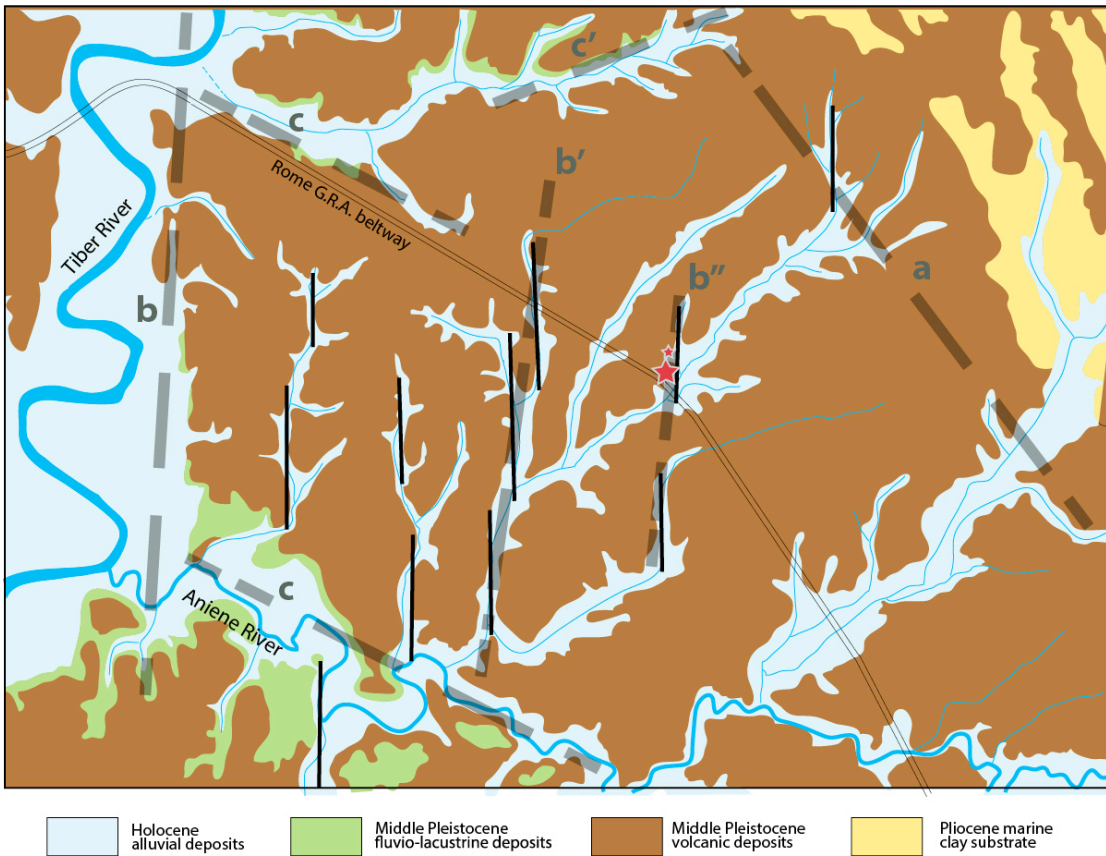


Figure 89. Geo-morpho-structural setting of the epicenter area. The thicker dashed lines represent the main buried faults inferred from the analysis of the hydrographic network, with the exception of the "a" fault, interpreted on the basis of the presence of a structural high to the NE, represented by outcrops of Pliocene sediments. A fourth set of NE-SW lineaments is likely originated by the topographic gradient in this area and is not highlighted as potential structural control. The thin, solid lines represent the superficial expression of the deformation linked to faults that are continuous at depth (b', b''), evidenced by straight tracts of the riverbeds. One of these deep NNE-SSW faults is the one that generated the May 11th earthquake, as the focal mechanism of this event suggests.

ii- The second set of lineaments has a direction from NS to NNE-SSW ("b" in Fig. 89) and reflects that of even older faults, with right-lateral strike-slip character (i.e. sub-vertical faults with right-hand horizontal movement (Alfonsi et al., 1991; Faccenna et al., 1994). These faults are linked to the dismemberment of the Apennine chain in independent arcs, due to the fragmentation of the "slab", that is the "Adriatic" tectonic plate which subducted below the Apennine orogenetic chain (Malinverno and Rayan, 1986; Patacca et al., 1990). However, these faults have been active until recent times (Faccenna et al., 2008; Marra et al., 2004b), probably due to the independent geodynamic mechanism that generated them, and are competing with the regime of forces that originated the extensional

561 faults (Marra, 2001; Faccenna et al., 1996). We also know from the analysis of the
 562 focal mechanisms of local earthquakes that small N-S fault segments are
 563 currently reactivated with opposite movement (left-lateral) together with the
 564 "Apennine", dip-slip faults (Frepoli et al., 2010).

565

566 iii- Finally, a third set of lineaments has conjugated WNW-ESE and ENE-WSW
 567 directions ("c" and "c'" in Fig. 89) and creates particular rhomboid "domains"⁹.
 568 Within these discrete regions, the N-S direction (as in the case of the epicenter
 569 area of the Rome's May 11th, 2020 earthquake, Fig. 89), or the same WNW-ESE
 570 directions (sectors 1A and 5A in Fig. 5B) may prevail. The origin of these
 571 domains is linked to the strike-slip faults and can be generated between two
 572 long, parallel N-S lineaments (Jones and Tanner, 1995). The characteristic of the
 573 strike-slip (transcurrent) faults is precisely that of being arranged in parallel
 574 with "en-echelon" geometry, that is, along stairway segments which can,
 575 however, locally have a lateral overlap between them (Sylvester, 1988). The en-
 576 echelon geometry characterizes the surface expression of faults that are
 577 continuous at depth (Sylvester, 1988) (examples b' and b" in Fig. 89).

578

579 **8. Conclusions**

580 The analysis of the hydrographic network in the epicenter area of the May 11th,
 581 2020 earthquake shows a relative maximum concentration of the streambed in
 582 the NNE-SSW direction: some of such rectilinear tracts, arranged with en-
 583 echelon geometry, are highlighted in Fig. 5. We interpret these features as the
 584 surface expression of buried NNE-SSW, strike-slip faults. Indeed, the focal
 585 mechanism and aftershock alignment reveal that one of these buried ~N-S fault
 586 reactivated with left-lateral movement on the occasion of the May 11th 2020
 587 earthquake. Effectively, tectonically sensitive geomorphic analyses revealed the
 588 occurrence of a cluster of knickpoints in the right side of the Aniene River that
 589 can be classified as slope-break knickpoints and are aligned along NW-SO and N-
 590 S orientation. Such a fluvial net perturbation corroborates the hypothesis of
 591 recent tectonic activity affecting the study area along those faults.

592 When we consider the multitude of lineaments that are present at a wider and at
 593 a smaller scale in this region (e.g., Fig. 2 and Fig. 89, respectively), we realize the

594 extreme fragmentation deriving from the intricate network of genetically
595 different faults. Such fragmentation results into a number of small fault
596 segments, with respect to the original long fault lines generated under the
597 competitive tectonic regimes that affected this region during Pleistocene times.

598 We remark that such high fragmentation is mainly provided by a en-echelon
599 system of ~N-S strike-slip faults which have crustal continuity. Therefore
600 hindering the lateral continuity of the NW-SE trending faults, which represent
601 the most favorably oriented fault system with respect to the Present-day NE-SW
602 extensional regime.

603 Small fault planes and a weaker tectonic regime explain the occurrence of
604 moderate seismicity and provide a likely explanation for the inhabitants of Rome
605 of the reason why they should not expect- that a large e~~a~~srthquake may affect the
606 City.

607

608

609 **Additional information**

610 The authors declare no competing financial and non-financial interests.

611

612 **Data availability statement**

613 All data generated or analyzed during this study are included in this published
614 article.

615

616 **Author Contribution statement**

617 F.M. conceptualization, methodology, validation, investigation, Writing - Original
618 draft, supervision
619 A.F. methodology, validation, investigation, data curation, Writing - Original draft
620 D.G. methodology, validation, investigation, data curation, Writing - Original draft
621 M.S. methodology, validation, investigation, data curation, Writing - Original
622 draft
623 A.T. methodology, validation, investigation, data curation, Writing - Original draft
624 M.B. methodology, validation, investigation, data curation, Writing - Review and
625 editing
626 G.D.L. methodology, validation, investigation, data curation, Writing - Review and
627 editing
628 M.L. methodology, validation, investigation, data curation, Writing - Review and
629 editing
630
631

632

633

634

635

636

637

638 REFERENCES

639

640 **Acocella, V., & Funiciello, R. (2006). Transverse systems along the extensional**
641 **Tyrrhenian margin of central Italy and their influence on volcanism. Tectonics,**
642 **25(2), TC2003.**

643

644 Alfonsi, L., Funiciello, R., Mattei, M., Girotti, O., Maiorani, A., Preite Martinez, M.,
645 Trudu, C., Turi, B.: Structural and geochemical features of the Sabina strike-slip
646 fault (Central Apennines), *Bollettino della Società Geologica Italiana*, 110, 217-
647 230, 1991.

648

649 **Amato, A., B. Alessandrini, G.B. Cimini, A. Frepoli, and G. Selvaggi, Active and**
650 **remnant subducted slabs beneath Italy: evidence from seismic tomography and**
651 **seismicity, Ann. Geofis., 36 (2), 201-214, 1993.**

652

653 Amato, A. and Chiarabba, C.: Earthquake occurrence and crustal structure, in:
654 The Volcano of the Alban Hills, edited by Trigila, R., Univ. degli Studi di Roma "La
655 Sapienza", Rome, 193-211, 1995.

656

657 Bahrami, S.: Analyzing the drainage system anomaly of zagros basins:
658 Implications for active tectonics, *Tectonophysics*, 608, 914-28, 2013.

659

660 Barberi, F., Buonasorte, G., Cioni, R., Fiordelisi, A., Foresi, L., Iaccarino, S.,
661 Laurenzi M.A., Sbrana, A., Vernia, L., Villa, I.M.: Plio-Pleistocene geological
662 evolution of the geothermal area of Tuscany and Latium, *Mem. Descr. Carta Geol.*
663 Ital., 49, 77-134, 1994.

664

665 Basili, A., Cantore, L., Cocco, M., Frepoli, A., Margheriti, L., Nostro, C., Selvaggi, G.:
666 The June 12, 1995 microearthquake sequence in the city of Rome, *Ann. Geofis.*,
667 39(6), 1167-1175, 1996.

668

669 Boulton, S.J., Stokes, M., Mather, A.E.: Transient fluvial incision as an indicator of
670 active faulting and Plio-Quaternary uplift of the Moroccan High Atlas,
671 *Tectonophysics*, 633, 16-33, doi: 10.1016/j.tecto.2014.06.032, 2014.

672

673 Calzolari, G., Della Seta, M., Rossetti, F., Nozaem, R., Vignaroli, G., Cosentino, D.,
674 Faccenna, F.: Geomorphic signal of active faulting at the northern edge of Lut
675 Block: Insights on the kinematic scenario of Central Iran, *Tectonics*, 35(1), 76-
676 102, doi: <https://doi.org/10.1002/2015TC0038692016>.

677

678 Caputo, C., Ciccacci, S., De Rita, D., Fredi, P., Lupia Palmieri, E., Salvini, F.: Drainage
679 pattern and tectonics in some volcanic areas of Latium (Italy), *Geologica Romana*,
680 29, 1-13, 1993.

681

682 Chatelain, J.L.: Etude fine de la sismicité en zone de collision continentale à l'aide
683 d'un réseau de stations portables: la region Hindu-Kush-Pamir. Thèse de 3 éme
684 cycle, Univ. Paul Sabatier, Toulouse, 1978.

685

- 686 Ciccacci, S., Fredi, P., Lupia Palmieri, E., Salvini, F.: An approach to the
 687 quantitative analysis of the relations between drainage pattern and fracture
 688 trend, in: International Geomorphology 1986, edited by Gardiner, V., Proceedings
 689 of the First International Conference on Geomorphology, Part II, John Wiley and
 690 Sons Ltd, Chichester, 49-68, 1987.
- 691
- 692 Del Monte, M., D'Orefice, M., Luberti, G.M., Marini, R., Pica, A., Vergari, F.:
 693 Geomorphological classification of urban landscapes: the case study of Rome
 694 (Italy), *Journal of Maps*, 12, 178-189, DOI:10.1080/17445647.2016.1187977,
 695 2016.
- 696
- 697 De Luca, G., Cattaneo, M., Monachesi, G., Amato, A.: Seismicity in central and
 698 northern Apennines integrating the Italian national and regional networks,
 699 *Tectonophysics*, 476(1), 121-135, doi:10.1016/j.tecto.2008.11, 2009.
- 700
- 701 Faccenna, C., Funiciello, R., Mattei, M.: Late Pleistocene N-S shear zones along the
 702 Latium Tyrrhenian margin: structural characters and volcanological
 703 implications, *Bollettino di Geofisica Teorica Applicata*, 36, 507-522, 1994a.
- 704
- 705 Faccenna, C., R. Funiciello, P. Montone, M. Parotto, and M. Voltaggio, An example
 706 of late Pleistocene strike-slip tectonics: the Acque Albule basin (Tivoli, Latium),
 707 *Mem. Descr. d. Carta Geol. d'It.*, 49, 37-50, 1994b.
- 708
- 709 Faccenna, C., Davy, P., Brun, J.P., Funiciello, R., Giardini, D., Mattei, M., Nalpas, T.:
 710 The dynamics of back-arc extension: an experimental approach to the opening
 711 of the Tyrrhenian Sea, *Geophysical Journal International*, 126, 781-795, 1996.
- 712
- 713 Faccenna, C., Soligo, M., Billi, A., De Filippis, L., Funiciello, R., Rossetti, C.,
 714 Tucciemei, P.: Late Pleistocene depositional cycles of the Lapis Tiburtinus
 715 travertine (Tivoli, Central Italy): Possible influence of climate and fault activity,
 716 *Global and Planetary Change*, 63(4), 299-308, 2008.
 717 doi:10.1016/j.gloplacha.2008.06.006
- 718
- 719 Forte, A.M. and Whipple, K.X.: Short communication: The Topographic Analysis
 720 Kit (TAK) for TopoToolbox, *Earth Surf Dynam*, 7(1), 87-95, doi: 10.5194/esurf-7-
 721 87-2019, 2019.
- 722
- 723 Frepoli, A., and A. Amato, Contemporaneous extension and compression in the
 724 northern Apennines from earthquake fault-plane solutions, *Geophys. J. Int.*, 129,
 725 368-388, 1997.
- 726
- 727 Frepoli A, Marra F, Maggi C, Marchetti A, Nardi A, Pagliuca NM, et al. Seismicity,
 728 seismogenic structures and crustal stress field in the greater area of Rome
 729 (Central Italy). *Journal Geophysical Research* 2010;115.
 730 doi:10.1029/2009JB006322, 2010
- 731
- 732 Frepoli, A., Cimini, G.B., De Gori, P., De Luca, G., Marchetti, A., Monna, S., Montuori,
 733 C., Pagliuca, N.: Seismic sequences and swarms in the Latium-Abruzzo-Molise
 734 Apennines (central Italy): new observations and analysis from a dense

- 735 monitoring of the recent activity, *Tectonophysics*, 712-713, 312-329,
 736 doi.org/10.1016/j.tecto.2017.05.026, 2017.
- 737
- 738 Galli, P.A.C. and Molin, D.: Beyond the damage threshold: the historic
 739 earthquakes of Rome, *Bull Earthquake Eng.*, 12, 1277-1306,
 740 https://doi.org/10.1007/s10518-012-9409-0, 2014.
- 741
- 742 Gaeta, M., Freda, C., Marra, F., Arienzo, I., Gozzi, F., Jicha, B., Di Rocco, T.: Paleozoic
 743 metasomatism at the origin of Mediterranean ultrapotassic magmas: constraints
 744 from time-dependent geochemistry of Colli Albani volcanic products (Central
 745 Italy), *Lithos*, 244, 151-164, 2016.
- 746
- 747 Gioia, D., Schiattarella, M., Giano, S.: Right-Angle Pattern of Minor Fluvial
 748 Networks from the Ionian Terraced Belt, Southern Italy: Passive Structural
 749 Control or Foreland Bending?, *Geosciences*, 8(9), 331, PubMed PMID,
 750 doi:10.3390/geosciences8090331, 2018.
- 751
- 752 Guidoboni, E., Ferrari, G., Mariotti, D., Comastri, A., Tarabusi, G., Sgattoni, G.,
 753 Valensise, G.: CFTI5Med, Catalogo dei Forti Terremoti in Italia (461 a.C.-
 754 1997) e nell'area Mediterranea (760 a.C.-1500), Istituto Nazionale di Geofisica
 755 e Vulcanologia (INGV), <http://storing.ingv.it/cfti5>, 2018.
- 756
- 757 Holland, J.H.: *Adaptation in Natural and artificial systems*, University of Michigan
 758 Press, Ann Arbor, 1975.
- 759
- 760 Horvath, F., and H. Berckhemer, Mediterranean back arc basins, in *Alpine*
 761 *Mediterranean Geodynamics*, pp. 145-175, eds Berckhemer, H. & Hsu, K.J.,
 762 *Geodyn. Ser.*, 7, American Geophys. Un., Whashington, DC., 1982.
- 763
- 764 Jones, R.R. and Tanner, P.W.G.: Strain partitioning in transpression zones, *Journal*
 765 *of Structural Geology*, 17, 793-802, 1995.
- 766
- 767 Kent, E., Boulton, S.J., Whittaker, A.C., Stewart, I.S., Cihat Alçıçek, M.: Normal fault
 768 growth and linkage in the Gediz (Alaşehir) Graben, Western Turkey, revealed by
 769 transient river long-profiles and slope-break knickpoints, *Earth Surface*
 770 *Processes and Landforms*, 42(5), 836-52, https://doi.org/10.1002/esp.4049,
 771 2017.
- 772
- 773 Kirby, E. and Whipple, K.X.: Expression of active tectonics in erosional
 774 landscapes, *Journal of Structural Geology*, 44:54-75,
 775 https://doi.org/10.1016/j.jsg.2012.07.009, 2012.
- 776
- 777 Lahr, J.C.: HYPOELLIPE/Version 2.0: a computer program for determining local
 778 earthquake hypocentral parameters, magnitude and first-motion pattern, U.S.
 779 *Geol. Surv. Open-file Report*, 95, 89-116, 1989.
- 780
- 781 Locardi, E., Lombardi, G., Funiciello, R., Parotto, M.: The Main volcanic groups of
 782 Latium (Italy): relations between structural evolution and petrogenesis,
 783 *Geologica Romana*, 15, 279-300, 1977.

- 784
- 785 Lucente, F.P., and F. Speranza, Belt bending driven by lateral bending of
786 subducting lithospheric slab: geophysical evidences from the northern
787 Apennines (Italy), *Tectonophysics*, 337, 53-64, 2001.
- 788
- 789 Macka, Z: Structural control on drainage network orientation an example from
790 the Loucka drainage basin, SE margin of the Bohemian Massif (S Moravia, Czech
791 Rep.), *Landform Analysis*, 4, 109-117, 2003.
- 792
- 793 Malinverno, A. and Ryan, W.B.F.: Extension in the Tyrrhenian sea and shortening
794 in the Apennines as results of arc migration driven by sinking of the lithosphere,
795 *Tectonics*, 5: 227-245, 1986.
- 796
- 797 Mariucci, M.T., A. Amato, and P. Montone, Recent tectonic evolution and present
798 stress in the Northern Apennines (Italy), *Tectonics*, 18, 108-118, 1999.
- 799
- 800 Marra, F.: Low-magnitude earthquakes in Rome: structural interpretation and
801 implications for local stress-field, *Geophysical Journal International*, 138, 231-
802 243, 1999.
- 803
- 804 Marra, F., Strike-slip faulting and block rotation: A possible triggering
805 mechanism for lava flows in the Alban Hills? *J. Struct. Geol.*, 23 (2), 129-141,
806 2001.
- 807
- 808 Marra, F., Taddeucci, J., Freda, C., Marzocchi, W., Scarlato, P.: Recurrence of
809 volcanic activity along the Roman Comagmatic Province (Tyrrhenian margin of
810 Italy) and its tectonic significance, *Tectonics*, 23, TC4013.
811 doi:10.1029/2003TC001600, 2004.
- 812
- 813 Marra, F., Montone, P., Pirro, M., Boschi, E.: Evidence of Active Tectonics on a
814 Roman Aqueduct System (II-III Century A.D.) near Rome, Italy, *Journal of Structural
815 Geology*, 26, 679-690, 2004.
- 816
- 817 Marra F., D.B. Karner, C. Freda, M. Gaeta, and P.R. Renne, Large mafic eruptions at
818 the Alban Hills Volcanic District (Central Italy): chronostratigraphy, petrography
819 and eruptive behavior, *J. Volc. Geoth. Res.* (in press),
820 doi:10.1016/j.jvolgeores.2008.11.009, 2009.
- 821
- 822 Marra, F., Sottili, G., Gaeta, M., Giaccio, B., Jicha, B., Masotta M., Palladino, D.: Major
823 explosive activity in the Sabatini Volcanic District (central Italy) over the 800-
824 390 ka interval: geochronological - geochemical overview and
825 tephrostratigraphic implications, *Quaternary Science Reviews*, 94, 74-101,
826 DOI:10.1016/j.quascirev.2014.04.010, 2014.
- 827
- 828 Marra, F., Florindo, F., Anzidei, M., Sepe, V.: Paleo-surfaces of glacio-eustatically
829 forced aggradational successions in the coastal area of Rome: assessing interplay
830 between tectonics and sea-level during the last ten interglacials, *Quaternary
831 Science Review*, 148: 85-100,
832 <http://dx.doi.org/10.1016/j.quascirev.2016.07.003>, 2016.

- 833
 834 Molin, D. and Rossi, A.: Effetti prodotti in Roma dai terremoti del 1703, in
 835 Settecento abruzzese, in: Eventi sismici, mutamenti economico-sociali e ricerca
 836 storiografica, edited by Colapietra, R., Marinangeli, G., Muzzi, P., L'Aquila, 69-106,
 837 2004.
- 838
 839 Montone, P, Amato A, Chiarabba C, Buonasorte G, Fiordelisi A, Evidence of active
 840 extension in Quaternary volcanoes of Central Italy from breakout analysis and
 841 seismicity, *Geophysical Research Letters* 1995;22: 1909-1912.
- 842
 843 Montone, P. and Mariucci, M.T.: The new release of the Italian contemporary
 844 stress map, *Geophysical Journal International*, 205(3), 1525-1531,
 845 doi:10.1093/gji/ggw100, 2016.
- 846
 847 Patacca, E., and P. Scandone, Post-Tortonian mountain building in the Apennines.
 848 The role of the passive sinking of a relic lithospheric slab, in *The Lithosphere in*
 849 *Italy*, edited by A. Boriani, M. Bonafede, G.B. Piccardo & G.B. Vai, *Advances in*
 850 *Earth Science Research. It. Nat. Comm. Int. Lith. Progr., Mid-term Conf. (Rome, 5-*
 851 *6 May 1987), Atti Conv. Lincei*, 80, 157-176, 1989.
- 852
 853 Patacca, E., Sartori, R., Scandone, P.: Tyrrhenian basin and apen- ninic arcs:
 854 Kinematic relations since late Tortonian times, *Mem. Soc. Geol. Ital.*, 45, 425-451,
 855 1990.
- 856
 857 Parotto, M. and Praturlon, A.: Geological summary of the Central Appenines, in:
 858 Structural Model of Italy, edited by Ogniben, L., Parotto, M., Praturlon A., *Quad.*
 859 *Ric. Scient.*, 90, 257-311, 1975.
- 860
 861 Pavano, F., Pazzaglia, F.J., Catalano, S.: Knickpoints as geomorphic markers of
 862 active tectonics: A case study from northeastern Sicily (southern Italy),
 863 *Lithosphere*, 8(6), 633-48, doi: 10.1130/L577.1, 2016.
- 864
 865 Peccerillo, A.: Cenozoic Volcanism in the Tyrrhenian Sea Region, S. IAVCEI,
 866 Barcelona, Springer, 2017.
- 867
 868 Reasenberg, P. and Oppenheimer, D.: FPFIT, FPPLOT and FPPAGE: FORTRAN
 869 computer programs for calculating and displaying earthquake fault plane
 870 solutions, *USGS Open-file Report*, 85-739, 1985.
- 871
 872 Reutter, K.J., P. Giese, and H. Closs, Lithospheric split in the descending plate:
 873 observation from the Northern apennines, *Tectonophysics*, 64, T1-T9, 1980.
- 874
 875 Rovida, A., Locati, M., Camassi, R., Lolli, B., Gasperini, P.: The Italian earthquake
 876 catalogue CPTI15. *Bulletin of Earthquake Engineering*, 18, 2953-2984.
 877 <https://link.springer.com/article/10.1007/s10518-020-00818-y>, 2020.
- 878
 879 Sambridge, M and Gallagher, K.: Earthquake hypocenter location using genetic
 880 algorithms, *Bull. Seism. Soc. Am.*, 83(5), 1467-1491, 1993.
- 881

- 882 Selvaggi, G., and A. Amato, Subcrustal earthquakes in the Northern Apennines
883 (Italy): evidence for a still active subduction? *Geoph. Res. Lett.*, 19, 2127-2130,
884 1992.
- 885
- 886 Serri, G., Neogene-Quaternary magmatic activity and its geodynamic implications
887 in the Central Mediterranean region, *Ann. Geofisica*, 3, 681-703, 1997.
- 888
- 889 Serri, G., F. Innocenti, and P. Manetti, Geochemical and Petrological evidence of
890 the subduction of delaminated Adriatic continental lithosphere in the genesis of
891 the Neogene-Quaternary magmatism of Central Italy, *Tectonophysics*, 223, 117-
892 147, 1993.
- 893
- 894 Tertulliani, A. and Riguzzi, F.: Earthquakes in Rome during the past one hundred
895 years, *Ann. Geofis.*, 38, 591-606, 1995.
- 896 Tertulliani A, Graziani L, Esposito A. How historical seismology can benefit from
897 bureaucracy: the case of the “Lettere Patenti” of the city of Rome in 1703. *Seism.*
898 *Res. Lett.* 2020;91, 2511-2519. <https://doi.org/10.1785/0220200046>
- 899
- 900 Trasatti, E., Marra, F., Polcari, M., Etiope, G., Ciotoli, G., Darrah, T., Tedesco, D.,
901 Florindo, F., Ventura, G.: Coeval uplift and subsidence reveal magma recharging
902 near Rome, *Geochemistry, Geophysics, Geosystems*.
903 DOI:10.1029/2017GC007303, 2018
- 904
- 905 Tveite, H.: The QGIS Line Direction Histogram Plugin,
906 <http://plugins.qgis.org/plugins/LineDirectionHistogram/>, 2015.
- 907
- 908 Whipple, K.X. and Tucker, G.E.: Dynamics of the stream-power river incision
909 model: Implications for height limits of mountain ranges, landscape response
910 timescales, and research needs, *Journal of Geophysical Research: Solid Earth.*,
911 104(B8),17661-74, doi: 10.1029/1999JB900120, 1999.
- 912
- 913 Wobus, C., Whipple, K.X., Kirby, E., Snyder, N., Johnson, J., Spyropolou, K., Crosby,
914 B., Sheehan, D.: Tectonics from topography: Procedures, promise, and pitfalls,
915 *Special Paper of the Geological Society of America*, 55-74, 2006.
- 916
- 917